Nonaffine rearrangements of atoms in deformed and quiescent binary glasses

Nikolai V. Priezjev
Department of Mechanical and Materials Engineering, Wright State University, Dayton, Ohio 45435, USA
(Received 1 May 2016; published 12 August 2016)

The influence of periodic shear deformation on nonaffine atomic displacements in an amorphous solid is examined via molecular dynamics simulations. We study the three-dimensional Kob-Andersen binary mixture model at a finite temperature. It is found that when the material is periodically strained, most of the atoms undergo repetitive nonaffine displacements with amplitudes that are broadly distributed. We show that particles with large amplitudes of nonaffine displacements are organized into compact clusters. With increasing strain amplitude, spatial correlations of nonaffine displacements become increasingly long-ranged, although they remain present even in a quiescent system due to thermal fluctuations.

DOI: 10.1103/PhysRevE.94.023004

I. INTRODUCTION

Elucidating the connection between atomic structure and mechanical properties of amorphous materials is important for a variety of optical and structural applications [1]. Unlike crystalline solids, where plasticity is determined by the motion of topological line defects called dislocations, an elementary process that leads to macroscopic plastic deformation of amorphous solids involves a collective rearrangement of a small number of atoms, often referred to as a shear transformation zone [2,3]. Hence, the localized plastic activity in a deformed material is associated with large nonaffine displacements of atoms, i.e., when atomic displacements do not match the macroscopic strain. Surprisingly, it was found that spatial correlations of nonaffine displacements in steadily sheared amorphous solids are long-ranged [4,5]. Recently, many experiments have been conducted to study shear-induced rearrangements of atoms and the yielding transition in glassy materials subjected to oscillatory shear strain [6–13]. However, the nature of spatial correlations of plasticity in glasses under periodic shear deformation remains not fully understood.

In the past few years, a number of studies have investigated the mechanical response of amorphous solids to oscillatory shear strain using atomistic quasistatic simulations in the athermal limit [14–17]. It was found that at small strain amplitudes, the systems evolve into periodic limit cycles where particles follow the same trajectories over consecutive cycles, and the number of cycles to reach a limit cycle increases as a critical strain amplitude is approached from below [15,17]. Interestingly, reversible avalanches of large particle displacements were observed at strain amplitudes below the critical value [17]. At finite temperatures, it was shown that the mean-square displacement of particles exhibits a broad subdiffusive plateau during 10 000 cycles even at small strain amplitudes, and the relaxation process involves intermittent clusters of particles undergoing cage jumps [18,19]. It was also found that at the critical strain amplitude, the number of mobile particles involved in a correlated motion reaches maximum [18,19].

The shear transformation zones were directly observed in recent experiments on colloidal glasses under reversible macroscopic shear deformation and at mechanical equilibrium [20]. The spatial correlations of the local strain field clearly showed the fourfold patterns, characteristic of Eshelby inclusions, that are present even in a quiescent system where their orientation is isotropic, thus producing zero global strain [20]. In turn, a local reversible shear transformation in a quiescent glass can trigger irreversible cage jumps whose density is large when the system dynamics is weakly damped or the shear transformation is slow [21,22]. More recently, a sharp transition from affine to nonaffine displacements of particles was identified in colloidal glasses under variable-amplitude oscillatory shear [6,7]. It was recently shown that during periodic deformation of binary glasses, particles undergo repetitive nonaffine displacements whose amplitudes become more broadly distributed with increasing strain amplitude [23]. However, the spatial organization and correlations of nonaffine displacements as well as their occurrence in a quiescent system were not explored in detail.

In this paper, molecular dynamics simulations are performed to study nonaffine atomic displacements in a three-dimensional binary mixture model subjected to slow periodic shear at a finite temperature. We show that the oscillatory deformation induces repetitive collective rearrangements of atoms that deviate significantly from the affine displacement field at large strain amplitudes. It is found that in a deformed material, the spatial correlations of nonaffine displacements are long-ranged, while they become short-ranged in a quiescent system, where nonaffine rearrangements are thermally activated.

The remainder of the paper is organized as follows. The details of molecular dynamics simulations are given in the next section. The numerical results for the oscillatory shear deformation and quiescent systems and an analysis of nonaffine rearrangements of atoms are presented in Sec. III. A summary is given in the final section.

II. MOLECULAR DYNAMICS SIMULATIONS

The molecular dynamics simulations were performed using the open-source LAMMPS numerical code developed at Sandia National Laboratories [24]. We use the standard Kob-Andersen model [25] of a binary Lennard-Jones glass. Our three-dimensional system consists of $N = 60\,000$ atoms confined in a periodic box, as shown in Fig. 1. Two types of atoms are considered, $\alpha,\beta = A,B$, which interact via the truncated LJ

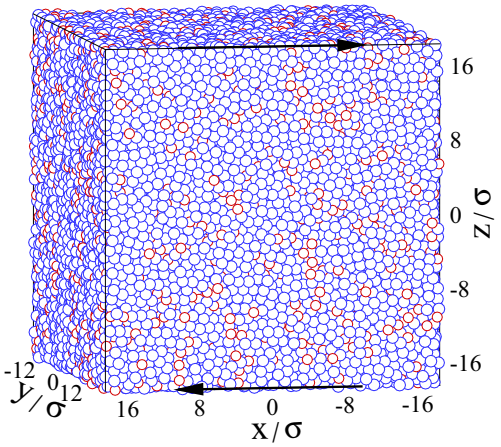

FIG. 1. The instantaneous atomic positions for a binary LJ glass annealed with a slow cooling rate of $10^{-5}\,\varepsilon/k_B\tau$ to the temperature $T_{\rm LJ} = 10^{-2}\,\varepsilon/k_B$. Atoms of type A are shown by large blue circles, and those of type B by small red circles. The arrows indicate the plane of periodic shear deformation.

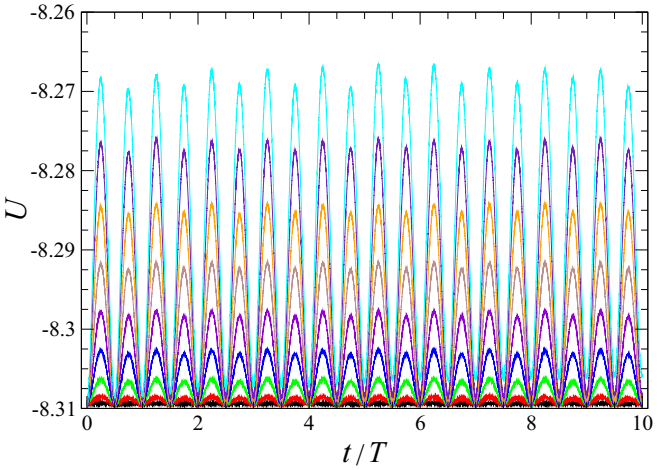

FIG. 2. The potential energy per atom U (in units of ε) during ten oscillation cycles for the strain amplitudes $\gamma_0 = 0$, 0.01, 0.02, 0.03, 0.04, 0.05, 0.06, 0.07, and 0.08 (from bottom to top).

potential as follows:

$$V_{\alpha\beta}(r) = 4\varepsilon_{\alpha\beta}\left[\left(\frac{\sigma_{\alpha\beta}}{r}\right)^{12} - \left(\frac{\sigma_{\alpha\beta}}{r}\right)^{6}\right], \qquad (1)$$

where the parameters are set to $\varepsilon_{AA} = 1.0$, $\varepsilon_{AB} = 1.5$, $\varepsilon_{BB} = 0.5$, $\sigma_{AB} = 0.8$, $\sigma_{BB} = 0.88$, and $m_A = m_B$ [25]. The cutoff radius is fixed to $r_{c,\,\alpha\beta} = 2.5\,\sigma_{\alpha\beta}$. As usual, the units of length, mass, and energy are set as $\sigma = \sigma_{AA}$, $m = m_A$, $\varepsilon = \varepsilon_{AA}$, and, correspondingly, the unit of time is $\tau = \sigma\sqrt{m/\varepsilon}$. The equations of motion were integrated using the Verlet algorithm [26] with the time step $\triangle t_{\rm MD} = 0.005\,\tau$.

The atoms were initially arranged at the sites of the face-centered-cubic lattice within a cubic box of linear dimension $L = 36.84\,\sigma$. Throughout the study, the density of atoms was kept constant, $\rho = \rho_A + \rho_B = 1.2\,\sigma^{-3}$. First, the system was equilibrated in the absence of deformation at the high temperature $1.1\,\varepsilon/k_B$, which is well above the computer glass transition temperature $T_g \approx 0.45\,\varepsilon/k_B$ [25]. Here, k_B denotes the Boltzmann constant. The temperature was controlled by the Nosé-Hoover thermostat with the damping time of 1.0τ. Then, the system was gradually cooled with a computationally slow rate of $10^{-5}\,\varepsilon/k_B\tau$ to the target temperature $T_{\rm LJ} = 10^{-2}\,\varepsilon/k_B$. This procedure was repeated for 20 independent samples.

The periodic shear strain deformation of the material was applied in the xz plane using the Lees-Edwards periodic boundary conditions [26], while the system remained periodic along the $\hat{y}$ direction. The shear strain was varied as a function of time according to

$$\gamma(t) = \gamma_0 \sin(2\pi t/T), \qquad (2)$$

where γ_0 is the strain amplitude and $T = 10^4\,\tau$ is the oscillation period. The corresponding oscillation frequency is $\omega = 2\pi/T = 6.28 \times 10^{-4}\,\tau^{-1}$. We note that the streaming velocity was subtracted from the local particle velocity to compute temperature in the Nosé-Hoover thermostat [24]. The system was subject to periodic deformation during 10 cycles, and the positions of all atoms were saved every $T/100 = 100\,\tau$. The analysis of nonaffine displacements was performed in 20 independent samples in the range of strain amplitudes $0 \leqslant \gamma_0 \leqslant 0.08$ during the last five cycles.

III. RESULTS

The time-periodic deformation of an amorphous solid typically involves an alternating sequence of elastic strain separated by rapid plastic events, which are accompanied by sudden drops in stress and the potential energy [17]. Depending on the strain amplitude, the local rearrangements of particles can be reversible after one or more cycles, or irreversible leading to chaotic system dynamics and particle diffusion [17]. In our study, the periodic shear strain is spatially homogeneous, which prevents the formation of shear bands during a slow, nearly quasistatic, deformation period $T = 10^4\,\tau$.

The potential energy per atom is plotted in Fig. 2 for one representative sample, which was deformed during ten back-and-forth cycles at different strain amplitudes. The horizontal black line at $U \approx -8.31\varepsilon$ corresponds to the potential energy measured in the quiescent system. Note that for each curve, the superimposed noise is caused by the thermal motion of atoms. At small strain amplitudes $\gamma_0 < 0.06$, the minima of the potential energy at the end of each cycle remain unchanged, whereas at large strain amplitudes $\gamma_0 \geqslant 0.06$, the potential energy increases over consecutive cycles. These results imply that during periodic shear deformation at small strain amplitudes, the system dynamics is reversible after each cycle. In contrast, with increasing strain amplitude, $\gamma_0 \geqslant 0.06$, some atoms undergo irreversible displacements leading to a progressive increase in the potential energy.

These conclusions are consistent with the energy landscape picture of sheared glasses, namely that a cycle of large shear strain rejuvenates the amorphous material by relocating the system to shallower energy minima [27]. Depending on the annealing procedure, it was also shown that a cycle with a small strain amplitude overages the glass by moving the system to deeper energy minima [27]. In our simulations, the decrease in the potential energy after several deformation

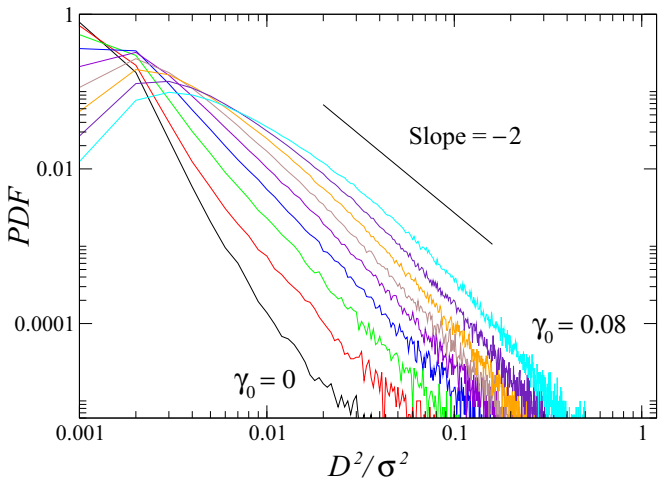

FIG. 3. The probability distribution function of $D^2(t,T/4)$ for the strain amplitudes $\gamma_0 = 0$, 0.01, 0.02, 0.03, 0.04, 0.05, 0.06, 0.07, and 0.08 (from left to right). The straight solid line indicates the slope −2.

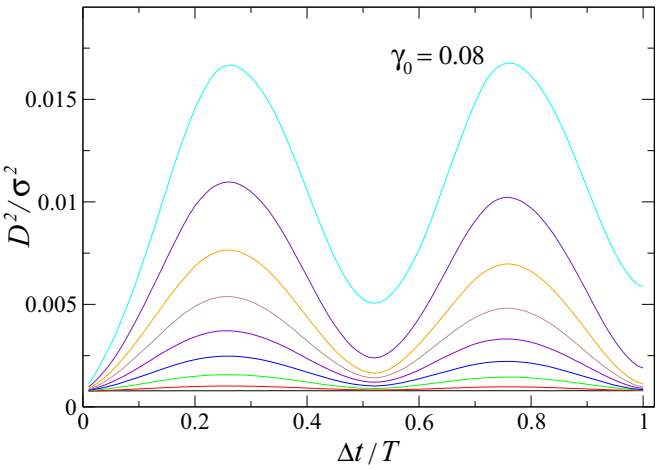

FIG. 4. Variation of the averaged quantity $D^2(t,\Delta t)$ during one oscillation period for the strain amplitudes $\gamma_0 = 0$, 0.01, 0.02, 0.03, 0.04, 0.05, 0.06, 0.07, and 0.08 (from bottom to top).

cycles is not observed at small strain amplitudes because of the computationally slow cooling rate that brings the system to an initial state with a very low energy minimum.

In general, during an affine deformation of the material, the displacement of atoms can be described by a combination of a linear transformation and a translation. Correspondingly, a deviation from the linear strain produces a finite nonaffine component of displacement of atoms with respect to their neighbors. The measure of the nonaffine displacement of the atom $\mathbf{r}_i(t)$ during the time interval Δt is defined as follows:

$$D^2(t,\Delta t) = \frac{1}{N_i}\sum_{j=1}^{N_i}\{\mathbf{r}_j(t+\Delta t) - \mathbf{r}_i(t+\Delta t) - \mathbf{J}_i\,[\mathbf{r}_j(t) - \mathbf{r}_i(t)]\}^2, \quad (3)$$

where the sum is taken over N_i nearest-neighbor atoms within the distance $1.5\,\sigma$ from $\mathbf{r}_i(t)$, and $\mathbf{J}_i$ is the transformation matrix that best maps all bonds between the ith atom and its nearest neighbors at times t and $t+\Delta t$ [3,28]. In the present study, the quantity $D^2(t,\Delta t)$ was computed every $100\,\tau$ during each cycle with respect to zero global strain.

In driven amorphous systems at finite temperatures, nonaffine rearrangements of atoms arise due to both external stresses and thermal fluctuations [29]. The normalized probability distribution function of nonaffine displacements is shown in Fig. 3 for various strain amplitudes. The quantity $D^2(t,\Delta t)$ was averaged over all atoms in 20 systems at the maximum strain $\Delta t = T/4$ with respect to zero strain. It can be seen that in the quiescent system, when $\gamma_0 = 0$, nonaffine deformations are present but their distribution is relatively narrow and bounded by $D^2(T/4) \approx 0.03\,\sigma^2$, which is comparable to the cage size $r_{\rm cage} \approx 0.1\,\sigma$. It should be noted that during the time interval $T/4$, the motion of nearest neighbors is uncorrelated, and therefore the quantity $D^2(T/4)$ essentially measures the average nonaffine rearrangement between two random configurations of atoms within their cages. One should recall that in a dense amorphous system at the low temperature $T_{\rm LJ} = 10^{-2}\,\varepsilon/k_B$, most of the atoms in the absence of external deformation remain within their cages, or escape only temporarily, on the time scale accessible to computer simulations [25].

With increasing strain amplitude, the probability distribution becomes more skewed toward larger values of $D^2(T/4)$ with the power-law exponent approaching −2 at the largest strain amplitude $\gamma_0 = 0.08$, as shown in Fig. 3. The nonaffine displacements of atoms with $D^2(T/4) \gg 0.01\,\sigma^2$ reflect the fact that their nearest-neighbor structure is significantly deformed during periodic strain. Moreover, the power-law distribution of $D^2(T/4)$ implies that highly nonaffine displacements are collectively organized, and, as will be shown below, they tend to form compact clusters. We further comment that the distribution functions shown in Fig. 3 change continuously near the critical strain amplitude $\gamma_0 = 0.06$, which marks the transition from a slow relaxation dynamics with a subdiffusive plateau to a diffusive regime [18,23]. Finally, it was also recently reported that the probability distribution function of $D^2(\Delta t)$, as well as other nonaffine measures based on displacement fluctuations and on deviation from the global deformation, exhibit a power-law decay with the slope −2.8 in steadily sheared colloidal glasses [4].

Next, we plot the variation of the quantity $D^2(t,\Delta t)$ in Fig. 4 during one oscillation period for the indicated strain amplitudes. The data were averaged over all atoms during the last five cycles. It can be observed that in the absence of external deformation, $D^2(t,\Delta t)$ is finite and time-independent. As mentioned above, nonaffine displacements in a quiescent system arise due to thermal vibration of atoms within their cages, and their local configurations become uncorrelated over time intervals $\Delta t \geqslant 0.01\,T = 100\,\tau$. Since the mean square displacement of atoms within their cages is proportional to temperature, it is expected that $D^2(\Delta t)$ scales as $T_{\rm LJ}$. Furthermore, as the strain amplitude increases, nonaffine displacements become more pronounced, especially near the maximum strain at $\Delta t = T/4$ and $3\,T/4$ (see Fig. 4). More importantly, the quantity $D^2(T)$ after a full cycle is greater than $D^2(0.01\,T)$ at large strain amplitudes $\gamma_0 \geqslant 0.06$, which

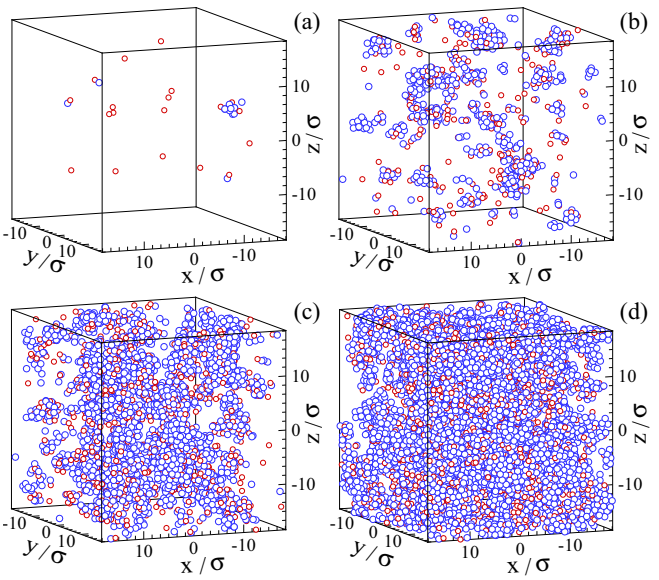

FIG. 5. Spatial configurations of atoms with large nonaffine displacements after a quarter of a cycle, $D^2(t,T/4) > 0.01\sigma^2$, for the strain amplitudes (a) $\gamma_0 = 0.00$, (b) $\gamma_0 = 0.02$, (c) $\gamma_0 = 0.04$, and (d) $\gamma_0 = 0.06$. The atoms of type A and B are denoted by blue and red circles, respectively.

implies that some atoms undergo irreversible displacements during one cycle. In marked contrast, at small strain amplitudes $\gamma_0 < 0.06$, the nonaffine measure $D^2(0.01\,T) \approx D^2(T)$, indicating reversible dynamics. This transition correlates well with the increase in the potential energy over consecutive cycles at $\gamma_0 \geqslant 0.06$ as shown in Fig. 2.

Figure 5 illustrates the spatial organization of atoms with large nonaffine displacements, $D^2(t,T/4) > 0.01\,\sigma^2$, for selected strain amplitudes. Notice that in the quiescent system, there are only several isolated atoms, mostly smaller atoms of type B, with large nonaffine components; although one group of atoms forms a small cluster [see Fig. 5(a)]. At the strain amplitude $\gamma_0 = 0.02$, localized regions of highly nonaffine displacements can be observed in Fig. 5(b). At larger strain amplitudes, $\gamma_0 = 0.04$ and 0.06, the clusters become interconnected and comparable with the system size. The appearance of repetitive clusters of atoms with large nonaffine displacements is consistent with reversible avalanches of particle rearrangements, which are associated with large drops in the potential energy, during periodic deformation of an athermal solid below the critical strain amplitude [17]. Moreover, it was also shown that energy drops are approximately power-law-distributed in a 2D solid under oscillatory shear below the yielding transition [17]. In our simulations, the cluster-size distribution was not computed due to insufficient statistics, since only several large clusters are typically present in each independent sample [23].

A related analysis of the spatial correlations of nonaffine displacements, however, can be performed by considering the normalized, equal-time correlation function [4,5,30] given by

$$C_{D^2}(\Delta\mathbf{r}) = \frac{\langle D^2(\mathbf{r}+\Delta\mathbf{r})D^2(\mathbf{r})\rangle - \langle D^2(\mathbf{r})\rangle^2}{\langle D^2(\mathbf{r})^2\rangle - \langle D^2(\mathbf{r})\rangle^2}, \qquad (4)$$

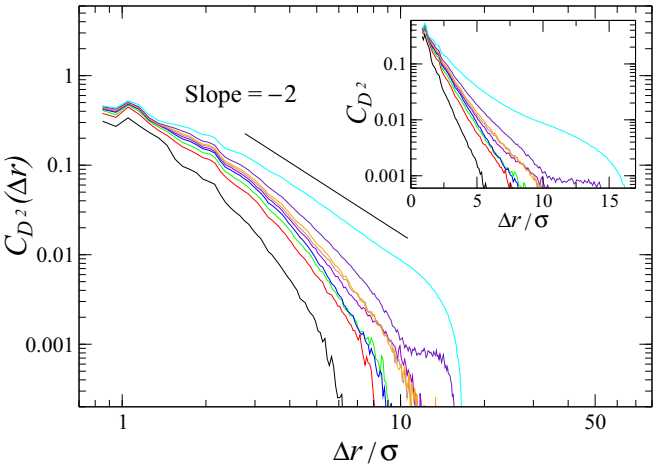

FIG. 6. The correlation function $C_{D^2}(\Delta\mathbf{r})$ defined by Eq. (4) for the strain amplitudes $\gamma_0 = 0$, 0.01, 0.02, 0.03, 0.04, 0.05, 0.06, 0.07, and 0.08 (from left to right). The straight line with the slope −2 is plotted for reference. The inset shows the same data on the log-normal scale.

where the angular brackets denote averaging over all pairs of atoms in 20 independent samples, and the quantity D^2 is computed at $\Delta t = T/4$ with respect to zero strain. The correlation function $C_{D^2}(\Delta\mathbf{r})$ is shown in Fig. 6 for quiescent and periodically strained glasses. It is clearly seen that with increasing strain amplitude, the spatial correlations become stronger and more long-ranged. At the largest strain amplitude $\gamma_0 = 0.08$, the data can be well described by a power-law decay with the exponent −2, followed by a cutoff due to the finite system size. As shown in the inset of Fig. 6, the decay of $C_{D^2}(\Delta\mathbf{r})$ at $\gamma_0 = 0$ is exponential, which indicates that correlations of thermally induced nonaffine rearrangements in a quiescent glass extend up to nearest-neighbor distances. Recently, it was pointed out that in steadily sheared glasses, spatial correlations of $D^2(\Delta\mathbf{r})$ at intermediate times change from an exponential to a power-law decay with the exponent of about −1.3 when the system size is increased [5]. In the present study, most of the rearrangements are reversible after one deformation cycle in a relatively large system, and the crossover from the exponential to the power-law decay of nonaffinity correlations occurs due to the increase in the strain amplitude.

IV. CONCLUSIONS

Using molecular dynamics simulations of a binary Lennard-Jones glass at a finite temperature, we have investigated the spatial distribution and correlation of plasticity in periodically strained and quiescent systems. In a three-dimensional amorphous glass, the nonaffine displacements were computed for each atom after multiple time intervals with respect to zero macroscopic strain. It was shown that nonaffine displacements arise both in quiescent and periodically deformed glasses. At mechanical equilibrium, the thermal motion of atoms within their cages leads to a relatively narrow distribution of nonaffine displacements, and their spatial correlations extend up to nearest-neighbor distances. During periodic deformation at

small strain amplitudes, nonaffine displacements are shear-induced, spatially heterogeneous, and reversible after each cycle. Above the critical strain amplitude, some atoms undergo irreversible nonaffine rearrangements, and the potential energy of the system increases over consecutive cycles. With increasing strain amplitude, nonaffine displacements become more broadly distributed and organized into large interconnected clusters. The numerical results indicate that spatial correlations of nonaffinity are approximately power-law distributed at large strain amplitudes.

In the future, it will be instructive to extend this study to larger systems and longer times in order to evaluate more accurately the cluster size distribution of nonaffine displacements and their spatial correlations, and to compare these results with experiments on periodically deformed colloidal glasses or bulk metallic glasses.

ACKNOWLEDGMENTS

Financial support from the National Science Foundation (Grant No. CNS-1531923) is gratefully acknowledged. The molecular dynamics simulations were conducted using the LAMMPS numerical code [24]. Computational work in support of this research was performed at Michigan State University's High Performance Computing Facility and the Ohio Supercomputer Center.

[1] T. C. Hufnagel, C. A. Schuh, and M. L. Falk, Acta Mater. **109**, 375 (2016).
[2] A. S. Argon, Acta Metall. **27**, 47 (1979).
[3] M. L. Falk and J. S. Langer, Phys. Rev. E **57**, 7192 (1998).
[4] V. Chikkadi and P. Schall, Phys. Rev. E **85**, 031402 (2012).
[5] F. Varnik, S. Mandal, V. Chikkadi, D. Denisov, P. Olsson, D. Vagberg, D. Raabe, and P. Schall, Phys. Rev. E **89**, 040301(R) (2014).
[6] D. V. Denisov, M. T. Dang, B. Struth, A. Zaccone, G. H. Wegdam, and P. Schall, Sci. Rep. **5**, 14359 (2015).
[7] M. T. Dang, D. Denisov, B. Struth, A. Zaccone, and P. Schall, Eur. Phys. J. E **39**, 44 (2016).
[8] M. Lundberg, K. Krishan, N. Xu, C. S. O'Hern, and M. Dennin, Phys. Rev. E **77**, 041505 (2008).
[9] K. N. Pham, G. Petekidis, D. Vlassopoulos, S. U. Egelhaaf, W. C. K. Poon, and P. N. Pusey, J. Rheol. **52**, 649 (2008).
[10] N. C. Keim and P. E. Arratia, Soft Matter **9**, 6222 (2013).
[11] E. D. Knowlton, D. J. Pine, and L. Cipelletti, Soft Matter **10**, 6931 (2014).
[12] M. C. Rogers, K. Chen, L. Andrzejewski, S. Narayanan, S. Ramakrishnan, R. L. Leheny, and J. L. Harden, Phys. Rev. E **90**, 062310 (2014).
[13] K. Hima Nagamanasa, S. Gokhale, A. K. Sood, and R. Ganapathy, Phys. Rev. E **89**, 062308 (2014).
[14] D. Fiocco, G. Foffi, and S. Sastry, Phys. Rev. E **88**, 020301(R) (2013).
[15] I. Regev, T. Lookman, and C. Reichhardt, Phys. Rev. E **88**, 062401 (2013).
[16] C. F. Schreck, R. S. Hoy, M. D. Shattuck, and C. S. O'Hern, Phys. Rev. E **88**, 052205 (2013).
[17] I. Regev, J. Weber, C. Reichhardt, K. A. Dahmen, and T. Lookman, Nat. Commun. **6**, 8805 (2015).
[18] N. V. Priezjev, Phys. Rev. E **87**, 052302 (2013).
[19] N. V. Priezjev, Phys. Rev. E **89**, 012601 (2014).
[20] K. E. Jensen, D. A. Weitz, and F. Spaepen, Phys. Rev. E **90**, 042305 (2014).
[21] N. V. Priezjev, Phys. Rev. E **91**, 032412 (2015).
[22] N. V. Priezjev, J. Phys.: Condens. Matter **27**, 435002 (2015).
[23] N. V. Priezjev, Phys. Rev. E **93**, 013001 (2016).
[24] S. J. Plimpton, J. Comput. Phys. **117**, 1 (1995); see also http://lammps.sandia.gov.
[25] W. Kob and H. C. Andersen, Phys. Rev. E **51**, 4626 (1995).
[26] M. P. Allen and D. J. Tildesley, *Computer Simulation of Liquids* (Clarendon, Oxford, 1987).
[27] D. J. Lacks and M. J. Osborne, Phys. Rev. Lett. **93**, 255501 (2004).
[28] J. Ding, Y. Q. Cheng, and E. Ma, Appl. Phys. Lett. **101**, 121917 (2012).
[29] D. M. Sussman, S. S. Schoenholz, Y. Xu, T. Still, A. G. Yodh, and A. J. Liu, Phys. Rev. E **92**, 022307 (2015).
[30] P. Murali, Y. W. Zhang, and H. J. Gao, Appl. Phys. Lett. **100**, 201901 (2012).